Available online at www.sciencedirect.com

ScienceDirect

journal homepage: www.jfda-online.com

Review Article

Applications of cyclic peptide nanotubes (cPNTs)

Wei-Hsien Hsieh [a], Jiahorng Liaw [b,*]

[a] Department of Biotechnology and Pharmaceutical Technology, Yuanpei University of Medical Technology, Hsinchu, Taiwan

[b] Department of Pharmaceutics, School of Pharmacy, College of Pharmacy, Taipei Medical University, Taipei, Taiwan

ARTICLE INFO

Article history:
Received 29 July 2018
Accepted 12 September 2018
Available online 28 September 2018

Keywords:
Cyclic peptide
Nanotube
Application

ABSTRACT

Self-assembled cyclic peptide nanotubes (cPNTs) have recently drawn particular attention as one of the most intriguing nanostructures in the field of nanotechnology. Given their unique features including high surface area, increased drug loading, environmental stability, enhanced permeation, and modifiable drug release, these hollow tubular structures can be constructed with cyclic di-, tri-, tetra-, hexa-, octa-, and decapeptides with various amino acid sequences, enantiomers, and functionalized side chains and can be applied for antiviral and antibacterial drugs, drug delivery and gene delivery vectors, organic electronic devices, and ionic or molecular channels. Recent publications have presented promising results regarding the use of cPNTs as drugs or biomedical devices. However, there is an urgent need for the further in vivo nanotoxicity and safety testing of these nanotubes to evaluate their suitability in different fields.

1. Introduction

Spherical nano- or microparticles, including liposomes, polymeric micelles, dendrimers, solid lipid nanoparticles, and inorganic nanoparticles, have been widely studied as drug carriers in recent decades to improve the effectiveness and efficiency of drugs [1]. To achieve targeting functionality and to control the distribution, circulation, elimination, and retention of these particles, the size and surface charge of these particles are important issues to consider [2,3]. Many studies have found that particles larger than 500 nm with a positive surface charge are easily distributed to reticuloendothelial systems such as the lung, spleen, liver, and lymph nodes via the phagocytotic pathway [2–4]. In addition to their size and surface properties, a geometric shape with a suitable aspect ratio (AR) and curvature is another key feature that strongly determines the intracellular uptake and biodistribution of particles [2,3]. Particles with a high AR of 22–60 μm length and 2–8 μm width were retained in the bloodstream 10 times longer than particles that are spherical [5,6]. These elongated structures within the "sweet spot" (1–20 μm in length) slow themselves momentum of the flow in the blood stream compared with spherical particles and reduce the number of cell membrane collisions [7]. Studies have successfully developed this type of nonspherical drug delivery system with long or extended half-life [3,7,8]. For example, Bruckman et al. [8] demonstrated that rod-shaped particles could still be observed in the liver and spleen

* *Corresponding author*. Fax: +8862 23779873.
E-mail address: jhorng@tmu.edu.tw (J. Liaw).

https://doi.org/10.1016/j.jfda.2018.09.004

24–96 h after administration compared with spherical particles. Furthermore, high-AR cylindrical particles with 150 nm diameter and 450 nm height (AR = 3) showed more rapid internalization by HeLa cells than 2 μm cubic particles, similar-volume low-AR cylindrical particles with 200 nm diameter and 200 nm height (AR = 1), and smaller-volume high-AR cylindrical particles with 100 nm diameter and 300 nm height (AR = 3) [2,9]. The easier internalization and nuclear distribution in cells of such high-AR cylindrical particles were suggested to be attributable to their larger surface areas that are in contact with the cell membrane [2,9]. The high surface area of nanotubes has also the potential to facilitate the delivery of drugs, peptides, and nucleic acids. These compounds can be encapsulated in multiple hollow cores of nanotubes, whereas other molecules can be attached to the external surfaces to render them dispersible and biocompatible for targeting purposes [7]. Therefore, nanotubes have been considered promising novel nanocarriers for drug delivery.

Many materials, such as carbon [10–14], silica [15], lipids [16,17], proteins [18,19], and peptides [20], have been discovered to form nanotubes that can be used for biological applications. Among them, carbon nanotubes (CNTs), which were discovered in 1991, were widely studied as molecular carriers for the delivery of drugs [10,11], proteins [12], and DNA [13,14]. On the basis of the characterization of ballistic conductance and their unique electronic structure, CNTs have been used for biosensors that rely on enzyme labels to generate electrical signals and perform hybridization or antigen–antibody interaction for the electrical detection of molecules, such as DNA [21] and cytochrome C [22], as well as biotin–streptavidin binding [23] and glucose oxidase activity [24]. However, safety concerns were raised about these approaches because of a number of reasons. For example, CNTs can cause inflammation [25,26], fibrosis, granuloma, and even death [27,28] in vivo when introduced into either the peritoneal cavity [25] or the lungs [26–28] of mice. Although the biocompatibility of silica nanotubes could be easily achieved by surface modification, the nonbiodegradable nature of these materials impedes their safety and hinders their development. As regards the unfavorable stability of lipids, there are certain factors that limit the application of lipid nanotubes, e.g., the ease of being directly taken up by the lymphatic system by Peyer's patches after the oral administration of these lipophilic micro- or nanocarriers [16] and the ease of morphological transformation by environmental calcium ions [17] that may affect the stability of carriers and inclusion molecules. Proteins are generally chemically unstable and are easily degraded by acidic pH, heat, enzymes, and oxidation. When protein-based nanotubes act as carriers and are administered orally, they are denatured at acidic pH because of pepsin in the stomach and then form large polypeptides and a negligible amount of free amino acids. These large polypeptides then enter the duodenum to be hydrolyzed by pancreatic proteolytic enzymes for absorption, thus resulting in the formation of free amino acids and short peptides with a chain length of two to six amino acid residues [29].

Compared with the above nanotubes, peptide nanotubes (PNTs) are considered simple, intrinsically biocompatible, and biodegradable materials with several attractive features. Therefore, PNTs have drawn increasing attention in recent years. One of the most attractive features of PNTs is their surface properties: their charge and hydrophobicity/hydrophilicity can be easily altered by changing the amino acids without additional chemical functionalization. This property provides greater versatility to tubular structures for the partial or complete encapsulation of a variety of hydrophobic/hydrophilic compounds in the hydrophobic interior and also confers targeting abilities [30]. For example, a homodimer L-diphenylalanine nanotube with a width of 0.7–10 μm and an AR greater than 50 was demonstrated by confocal microscopy to be stably loaded with a hydrophobic flufenamic acid molecule [31] and thioflavin [30,31]. By using pyrene that exhibits hydrophobicity, which is a well-known property that reflects microenvironmental polarity, we found that the predominant interactions involved in the hydrophobic pyrene–PNT complex included van der Waals and hydrophobic binding [32]. However, noninclusion complexes such as those with external hydrogen bonding affected by the ring strain in PNTs could also affect the release of hydrophilic drugs. For example, Silva et al. [20] found that a hydrophilic rhodamine B (RhB) molecule could interact with the polar group of a PNT matrix and demonstrated that molecules with two different properties could colocalize with PNTs. Furthermore, PNTs have been found to form noninclusion complexes not only with small-molecule drugs but also with macromolecules such as DNA. In our previous studies, we successfully included 3×10^{10} copies of plasmid DNA/mg in cyclo-(D-Trp-Tyr) PNTs with a binding constant of 3.2×10^{8} M^{-1} and 1.2 M fractions of DNA bound to Tyr residues in PNTs [32].

PNTs can be divided into two categories: one category is composed of linear peptides [33–35], and the other is composed of cyclic peptides (cPNTs) [34–36]. Owing to the ease of controlling the size of the radius of nanotubes and their surface properties by altering the amount and type of amino acids, pH, or polymeric conjugation, cPNTs were considered to be well-functional materials and devices in the fields of biochemistry, chemistry, biology, materials science, and medicine [37]. To date, three types of cPNT structures have been presented: cyclic D,L-α-peptides, cyclic β-peptides, and cyclic α-γ-peptides; it was shown that these could stack into tubular structures (Fig. 1) [36]. Cyclic D,L-α-peptides were the first to be discovered, which was achieved by Ghadiri et al. [36,38] in 1993. Under acidified conditions, the amino acid side chain in these peptides diverges outward, and the amide and carbonyl groups run perpendicular to the ring axis before finally forming an antiparallel β-sheet tubular structure via self-assembly (Fig. 1A) [36,38]. The self-assembling properties of cyclic β-peptides were subsequently shown to be similar to those of cyclic D,L-α-peptides, and the amino acid side chain radiates equatorially from the peptide ring. However, the orientation of the amide and carbonyl groups presents an opposite unidirectional allocation along the longitudinal axis of the tube, thus forming parallel stacking (Fig. 1B) [36,39]. The third type of cPNTs constructed by cyclic α-γ-peptides differs from those of cyclic D,L-α-peptides and cyclic β-peptides and has nonequivalent faced rings that stack flat together with different hydrogen bonding patterns as γ–γ and α–α interactions (Fig. 1C) [36,40]. The key aim of this review is to present an update of the application of these three types of

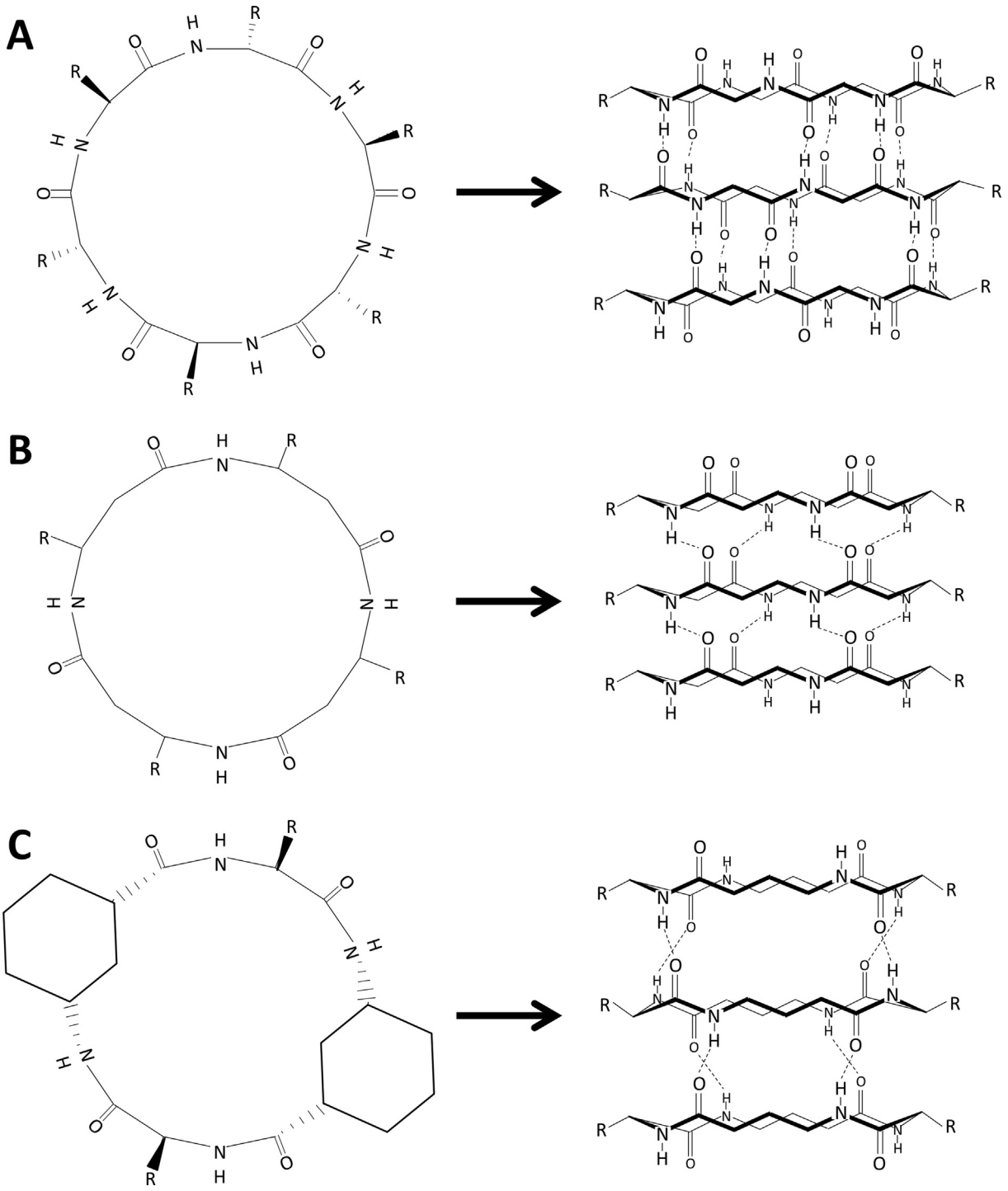

Fig. 1 – Categories of cyclic peptide nanotubes (cPNTs) by β-sheet stacking. The N–H and C=O hydrogen bond donors and acceptors are aligned with tube length in each case of (A) Cyclic D,L-α-peptides, (B) Cyclic β-peptides, and (C) Cyclic α-γ-peptides. (modified from Fig. 1 in referecne [36])

cPNT with respect to amino acid sequence, enantiomer, and ring size.

The cyclization of cPNTs and the incorporation of D-amino acids were frequently found to protect the inclusion molecules against biological pH and proteolytic degradation by conformational control or steric hindrance, which could provide stable shuttles [41,42]. For example, Samanen et al. [43] demonstrated that a cyclic analog of RGD peptide could maintain its anticoagulative activity for over 3 h, which was significantly superior to that of its linear analog. Similarly, our

previous study demonstrated that plasmid DNA with stable cPNTs that were constructed by cyclic D-Trp-Tyr could be protected against digestion by DNase I, acid, and bile for 50, 60, and 180 min, respectively, which were longer periods than for unloaded ones [32]. Furthermore, the degree of N-methylation of cyclic peptides could also dominate the metabolic enzyme stabilities of cPNTs, thus enhancing bioavailability [42,44]. The enhancement of stability by N-methylation may be attributable to the prevention of cleavage at N-terminal D-Trp, Lys, and Phe positions [44,45]. Moreover, the size of the vehicle is another factor that can influence stability. Geng et al. [5] found that high-AR vehicles with lengths greater than 8 μm could persist in circulation longer (for up to one week) than those with shorter lengths after IV injection in mice because of the slow cellular uptake under fluid flow conditions. A further study on the single tail-vein injection of paclitaxel, which is a hydrophobic anticancer drug, complexed with 8 μm-long filomicelles in mice showed the benefit of long stability in circulation, namely, the increased exposure of cancer cells to drugs as a result of effectively diminishing the tumor size compared with the administration of unloaded paclitaxel [5,46].

In addition to stability, the enhancement of permeability is another feature that enables cPNTs to deliver molecules and achieve high bioavailability. However, there are no consistent guidelines for the design of highly permeable cPNTs because of the existence of various uptake mechanisms involved in the absorption process, including passive transport and active transport [42]. Nonetheless, there are some rules of thumb related to the physiological cell absorption process; surface properties; and molecular weight, size, and shape, and these rules could be valuable. Fernandez-Lopez et al. [47] proposed several intriguing mechanisms, namely, intramolecular pore, barrel stave, and carpet models, to explain the passive transport of cPNTs. Among these three models, the carpet model was thought to have greater potential for involvement in membrane permeation because of its polyvalent display of surface-exposed hydrophilic side chains for potential interactions with various membrane constituents; this property has been proved by coarse-grained molecular dynamics (MD) simulation [47,48]. On the contrary, larger particles generally enter cells via an energy-dependent route, including endocytosis or phagocytosis [49]. Similarly, our previous study showed that plasmid DNA complexed with high-AR cyclo-(D-Trp-Tyr) PNTs with a width of 100–800 nm and a length of 1–20 μm could enhance the permeability of plasmid DNA for in vitro duodenal permeation, which involves an energy-dependent mechanism [32]. Therefore, well-designed high-AR cPNT vehicles could provide a versatile route for enhancing membrane absorption by either a passive or an active pathway.

The sustained release of guest molecules via their incorporation into cPNT carriers by electrostatic interaction, hydrogen binding, or hydrophobic interaction is also an attractive feature for biological applications. For example, the inclusion of small-molecule RhB into diphenylalanine PNTs resulted in slower release following first-order kinetics compared with RhB alone [20]. Flufenamic acid is another small-molecule model that has revealed the sustained-release properties of diphenylalanine PNT complexation [31]. Similar results were also observed in cPNTs complexed with large molecules, such as DNA. For example, our previous study showed that the release rate of DNA was 3.57×10^{11} copies DNA/$t^{1/2}$ with cyclo-(D-Trp-Tyr) PNT complexation, whereas that of unformulated DNA was faster at a rate of 5.92×10^{11} copies DNA/$t^{1/2}$ [32].

2. Biomedical applications

2.1. *Antiviral effects*

cPNTs constructed with an even number of alternating D- and L-α-amino acids have been demonstrated to exert antiviral activity. The antiviral spectrum, including envelope and nonenvelope viruses, is predominantly determined by the sequence of peptides. In general, the hydrophobicity of cPNTs was thought to affect the affiliation of cPNTs with the cell membrane, which affects the final activity. Hore et al. [50] found that an eight-residue cyclic D,L-α-peptide, cyclo-(Ser-D-His-Lys-D-Arg-Lys-D-Trp-Leu-D-Trp) (code 1) with antitype A influenza viral activity and IC_{50} of 5 μM (Table 1) acts by preventing HeLa cells from forming low-pH endocytic vehicles and further inhibiting viral escape from endosomes. Compared with cyclo-(Ser-D-His-Lys-D-Arg-Lys-D-Trp-Leu-D-Trp) (code 1) as a template, the reverse (code 2) and enantiomeric sequences (code 3) revealed similar IC_{50}, thus indicating that its antiviral activities may not involve a receptor/ligand-mediated mechanism. Furthermore, single-alanine-substitution analogs (codes 4–11) of the code 1 sequence also maintained the mode of action (Table 1). However, by changing the amino acid sequence or hydrophobicity of amino acids, a versatile range of cPNT interactions with the cell membrane can be induced to influence the activity. For example, a single substitution from tryptophan to alanine (codes 4 and 5) may diminish the hydrophobicity for membrane interaction, thus resulting in the abolition of activity. It was suggested that membrane partition is primarily mediated by a hydrophobic side chain, whereas membrane selectivity can be greatly affected by the interaction of a hydrophilic side chain with the cell membrane (Table 1) [50]. Motero et al. [51] screened 144 nontoxic cyclic D,L-α-peptide sequences with LD_{50} of more than 100 μM for HeLa cells in an attempt to discover antiviral activities against hepatitis C virus and to probe the structure–activity relationship. They found that amphiphilic net natural charge and the amino acid sequence strongly affects the antiviral activities (codes 12–27). For example, when assigning the code 12 sequence as a template, the reversal of the positions of a lysine/ornithine and glutamic acid pair to place one or two (codes 13 and 14) negatively charged glutamic acid residues in a hydrophobic region significantly reduced the activity (IC_{50}: 18–50 μM) (Table 1). Furthermore, peptide sequences of codes 15 and 16 are N-methylated analogs of code 17 designed to prohibit peptide stacking via intermolecular hydrogen binding. The IC_{50} of code 15 and 16 sequences significantly increased compared with that of the unmethylated one (code 17), thus suggesting that the self-assembly of cPNTs into supramolecular structures is required for antiviral activity and that they may interact with the lipid membrane owing to the relatively hydrophobic surface of the tubular structure (Table 1).

Table 1 – *In vitro* anti-viral and bacterial activities of cyclic D,L-α-peptide nanotubes (cPNTs).

Code	Cyclic Peptide Sequence	Anti-Virus Activity			Reference
		IC_{50} (μM)		LD_{50} (μM)	
		Type-A influenza	Hepatitis C	Hela cell	
1	Ser-D-His-Lys-D-Arg-Lys-D-Trp-Leu-D-Trp	5	ND	57	[50]
2	D-Trp-Leu-D-Trp-Lys-D-Arg-Lys-D-His-Ser	5	ND	35	
3	D-Ser-His-D-Lys-Arg-D-Lys-Trp-D-Leu-Trp	7	ND	63	
4	Ser-D-His-Lys-D-Arg-Lys-D-Ala-Leu-D-Trp	>30	ND	>100	
5	Ser-D-His-Lys-D-Arg-Lys-D-Trp-Leu-D-Ala	>30	ND	>100	
6	Ala-D-His-Lys-D-Arg-Lys-D-Trp-Leu-D-Trp	8	ND	54	
7	Ala-D-Ser-Lys-D-Arg-Lys-D-Trp-Leu-D-Trp	13	ND	70	
8	Ser-D-His-Ala-D-Arg-Lys-D-Trp-Leu-D-Trp	19	ND	>100	
9	Ser-D-His-Lys-D-Ala-Lys-D-Trp-Leu-D-Trp	7	ND	65	
10	Ser-D-His-Lys-D-Arg-Ala-D-Trp-Leu-D-Trp	6	ND	43	
11	Ser-D-His-Lys-D-Arg-Lys-D-Trp-Ala-D-Trp	17	ND	100	
12	D-Trp-Leu-D-Trp-Orn-D-Glu-Asn-D-Glu-Lys	ND	11	>100	[51]
13	D-Trp-Leu-D-Trp-Glu-D-Orn-Asn-D-Lys-Glu	ND	>50	>100	
14	D-Trp-Leu-D-Trp-Glu-D-Orn-Asn-D-Glu-Lys	ND	18	>100	
15	D-Trp-Leu^{Me}-D-Trp-Ser-D-Glu-Asn-D-Ser^{Me}-Lys	ND	>50	ND	
16	D-Trp-Leu^{Me}-D-Trp-Ser^{Me}-D-Glu-Asn-D-Ser-Lys	ND	>50	ND	
17	D-Trp-Leu-D-Trp-Ser-D-Glu-Asn-D-Ser-Lys	ND	7	>100	
18	D-Trp-Leu-D-Trp-Ser-D-Glu-Gln-D-Ser-Lys	ND	3	65	
19	D-Trp-Leu-D-Trp-Ser-D-Glu-Lys-D-Asn-Ser	ND	8	>100	[51]
20	D-Trp-Leu-D-Trp-Ser-D-Ser-Lys-D-Glu-Asn	ND	8	>100	
21	D-Trp-Leu-D-Trp-Ser-D-Glu-Gln-D-Ser-Orn	ND	10	>100	
22	D-Trp-Leu-D-Trp-Arg-D-Glu-Gln-D-Glu-Arg	ND	16	>100	
23	D-Trp-Leu-D-Tyr-Lys-D-Arg-Glu-D-Asp-Tyr	ND	9	>100	
24	D-Trp-Leu-D-Trp-DPA-D-Glu-Gln-D-Glu-DPA	ND	7	80	
25	D-Trp-Leu-D-Trp-Arg-D-Glu-Ser-D-Gln-Lys	ND	3	90	
26	D-Trp-Leu-D-Trp-Orn-D-Ser-Asn-D-Glu-Ser	ND	8	>100	
27	D-Trp-Ile-D-Trp-Orn-D-Glu-Asn-D-Glu-Lys	ND	6	45	

Code	Cyclic Peptide Sequence	Anti-Bacterial Activity								Reference
		MIC (μM)							HD_{50} (μM)	
		S. aureus	MRSA	E. Coli	U. Linza	N. Perminuta	B. Cereus	VRE	RBC	
28	D-Ser-Lys-D-Ser-Trp-D-Leu-Trp-D-Leu-Trp	ND	8	8	ND	ND	ND	ND	24	[47]
29	D-Thr-His-D-Ser-Trp-D-Leu-Trp-D-Leu-Trp	ND	80	80	ND	ND	ND	ND	80	
30	D-Ser-Lys-D-His-Trp-D-Leu-Trp-D-Leu-Trp	ND	12	78	ND	ND	ND	ND	16	
31	D-Glu-Lys-D-His-Trp-D-Leu-Trp-D-Leu-Trp	ND	76	76	ND	ND	ND	ND	76	
32	D-Lys-Lys-D-Lys-Trp-D-Leu-Trp-D-Leu-Trp	ND	6	53	ND	ND	ND	ND	38	
33	D-Arg-Arg-D-Lys-Trp-D-Leu-Trp-D-Leu-Trp	ND	4	11	ND	ND	ND	ND	37	
34	D-Lys-Arg-D-Lys-Trp-D-Leu-Trp-D-Leu-Trp	ND	7	30	ND	ND	ND	ND	37	[47]
35	D-Arg-Arg-D-Arg-Trp-D-Leu-Trp-D-Leu-Trp	ND	7	36	ND	ND	ND	ND	25	
36	D-His-Lys-D-His-Trp-D-Leu-Trp-D-Leu-Trp	ND	9	11	ND	ND	ND	ND	19	
37	D-Lys-His-D-Lys-Trp-D-Leu-Trp-D-Leu-Trp	ND	8	61	ND	ND	ND	ND	23	
38	D-Lys-Lys-D-Leu-Trp-D-Leu-Trp	ND	10	18	ND	ND	ND	ND	83	
39	D-Lys-His-D-Leu-Trp-D-Leu-Trp	ND	10	103	ND	ND	ND	ND	26	
40	D-Lys-Ser-D-Leu-Trp-D-Leu-Trp	ND	81	109	ND	ND	ND	ND	98	
41	D-Arg-Arg-D-Leu-Trp-D-Leu-Trp	ND	34	5	ND	ND	ND	ND	88	
42	D-Arg-Gly-D-Asp-Trp-D-Leu-Trp-D-Leu-Trp	ND	80	80	ND	ND	ND	ND	80	
43	D-Lys-Gln-D-Arg-Trp-D-Leu-Trp-D-Leu-Trp	ND	4	60	ND	ND	ND	ND	34	
44	Lys-D-Gln-Arg-D-Trp-Leu-D-Trp-Leu-D-Trp	ND	6	60	ND	ND	ND	ND	30	
45	D-Arg-Gln-D-Arg-Trp-D-Leu-Trp-D-Leu-Trp	ND	13	66	ND	ND	ND	ND	18	
46	D-Lys-Gln-D-Lys-Trp-D-Leu-Trp-D-Leu-Trp	ND	34	76	ND	ND	ND	ND	38	
47	D-Lys-Ser-D-Lys-Trp-D-Leu-Trp-D-Leu-Trp	ND	4	31	ND	ND	ND	ND	79	
48	D-Ser-His-D-Lys-Trp-D-Leu-Trp-D-Leu-Trp	ND	8	78	ND	ND	ND	ND	27	
49	D-Ser-His-D-His-Trp-D-Leu-Trp-D-Leu-Trp	ND	16	78	ND	ND	ND	ND	16	

Table 1 – (*continued*)

Code	Cyclic Peptide Sequence	Anti-Bacterial Activity								Reference
		MIC (μM)							HD_{50} (μM)	
		S. *aureus*	MRSA	E. Coli	U. Linza	N. Perminuta	B. Cereus	VRE	RBC	
50	D-Lys-Trp-D-Phe-His-D-Trp-Lys	ND	30	15	10	20	ND	ND	>100	[52]
51	Lys-D-Trp-Phe-D-His-Trp-D-Lys	ND	>100	7.5	12.5	ND	ND	ND	ND	
52	Lys-D-Trp-Trp-D-Phe-Trp-D-Lys	ND	30	100	10	40	ND	ND	>100	
53	Lys-D-Trp-Phe-D-Trp-Trp-D-Lys	ND	100	>100	30	20	ND	ND	>100	
54	Lys-D-Trp-Phe-D-Phe-Leu-D-His	ND	10	>100	10	>100	ND	ND	>100	
55	Lys-D-Trp-Leu-D-Phe-Phe-D-Lys	ND	7.5	40	40	20	ND	ND	50	
56	D-His-Trp-D-Phe-His-D-Trp-Lys	ND	15	20	50	20	ND	ND	>100	
57	D-Arg-Trp-D-Phe-His-D-Trp-Lys	ND	30	20	10	30	ND	ND	>100	
58	D-Ser-Trp-D-Phe-His-D-Trp-Lys	ND	10	40	5	8	ND	ND	>100	
59	D-Leu-Trp-D-Phe-His-D-Trp-Lys	ND	10	>100	>100	>100	ND	ND	>100	
60	D-Trp-Trp-D-Phe-His-D-Trp-Lys	ND	>100	>100	>100	>100	ND	ND	>100	
61	D-Tyr-Trp-D-Phe-His-D-Trp-Lys	ND	>100	>100	>100	>100	ND	ND	>100	
62	D-Phe-Trp-D-Phe-His-D-Trp-Lys	ND	>100	>100	>100	>100	ND	ND	>100	
63	Lys-D-Trp-Phe-D-Phe-Phe-D-His	ND	100	>100	1	100	ND	ND	>100	
64	Lys-D-Trp-Phe-D-Phe-Trp-D-His	ND	50	>100	30	>100	ND	ND	>100	
65	Lys-D-Trp-Phe-D-Phe-Lys-D-His	ND	15	10	10	8	ND	ND	>100	
66	Lys-D-Trp-Phe-D-Phe-His-D-His	ND	7.5	50	8	10	ND	ND	90	
67	Lys-D-Trp-Phe-D-Phe-Ser-D-His	ND	40	50	5	30	ND	ND	>100	
68	Lys-D-Trp-Phe-D-Lys-Trp-D-Ser	ND	>100	>100	50	30	ND	ND	>100	[52]
69	Lys-D-Trp-Phe-D-Lys-Lys-D-Leu	ND	50	20	>100	30	ND	ND	>100	
70	Lys-D-Trp-Phe-D-Leu-Trp-D-His	ND	100	>100	>100	40	ND	ND	>100	
71	Ser-D-Trp-Phe-D-Lys-Thr-D-Lys-Ser-D-Lys	7	ND	ND	ND	ND	ND	ND	>352	[53]
72	D-Ser-Trp-D-Phe-Lys-D-Thr-Lys-D-Ser-Lys	7	ND	ND	ND	ND	ND	ND	>352	
73	Ser-D-Trp-Phe-D-Lys-His-D-Lys-Ser-D-Lys	10	ND	ND	ND	ND	ND	ND	>341	
74	Ser-D-Trp-Asx-Tyr-D-Lys-Asn-D-Lys-Ser-D-Lys	2	ND	ND	ND	ND	ND	ND	161	
75	Ile-Leu-D-Trp-His-D-Orn-Lys	2	ND	ND	ND	ND	ND	ND	211	
76	D-Lys-Lys-D-His-Lys-D-Trp-Leu-D-Trp-Lys	2	ND	ND	ND	ND	ND	ND	79	
77	Trp-D-Leu-Trp-D-Lys-Ser-D-Lys-Ser-D-Ser(βGlcNH2)	ND	5	ND	ND	ND	10	10	65	[54]
78	Trp-D-Leu-Trp-D-Lys-Ser-D-Ser(βGlcNH2)-Ser-D-Lys	ND	5	ND	ND	ND	10	10	90	
79	Trp-D-Leu-Trp-D-Ser(βGlcNH2)-Ser-D-Lys-Ser-D-Lys	ND	5	ND	ND	ND	15	10	80	
80	Trp-D-Leu-Trp-D-Lys-Ser-D-Lys-Ser(βGal)-D-Lys	ND	5	ND	ND	ND	10	15	150	
81	Trp-D-Leu-Trp-D-Lys-Ser(βGal)-D-Lys-Ser-D-Lys	ND	5	ND	ND	ND	5	10	105	
82	Trp-D-Leu-Trp-D-Lys-Ser-D-Lys-Ser(αMan)-D-Lys	ND	2.5	ND	ND	ND	10	10	70	
83	Trp-D-Leu-Trp-D-Lys-Ser(αMan)-D-Lys-Ser-D-Lys	ND	2.5	ND	ND	ND	5	5	50	
84	Trp-D-Leu-Trp-D-Lys-Ser-D-Lys-Ser-D-Lys	ND	5	ND	ND	ND	5	10	65	

The cytotoxicity expressed by LD50 was evaluated by MTT assay or XTT assay. Me: N-Methylation; ND: Non-detected; DPA: 2,3-Diaminopropionic acid; MIC: Minimum inhibition concentration; HD: Hemolytic dose; MRSA: Methicillin-resistant *Staphylococcus aureus* (ATCC33591); VRE: Vancomycin-resistant *Enterococcus faecalis* (ATCC51575); RBC: Red blood cell.

2.2. *Antibacterial effects*

Superbacteria with antibiotic resistance due to the misuse of antibiotics have attracted attention in recent decades. There is a growing need for antimicrobial agents with novel mechanisms of action to combat such bacteria. In this context, Fernandez-Lopez et al. [47] demonstrated in 2001 that six- and eight-residue amphipathic cyclic D,L-α-peptides with appropriate amino acid sequences for stacking into hollow and β-sheet-like cPNT structures bearing suitable outer surface properties could potentially act against either gram-positive or gram-negative bacteria; it was proposed that this involves a carpet-like mechanism that enhances membrane permeability and causes rapid cell death. For example, the sequence cyclo-(D-Ser-Lys-D-Ser-Trp-D-Leu-Trp-D-Leu-Trp) (code 28) was found to be effective against methicillin-resistant *Staphylococcus aureus* (MRSA) and *Enterococcus coli* (*E. coli*) with a minimum inhibitory concentration (MIC) of 8 μM for each (Table 1) in vitro [47]. Similar to the results in the previous antivirus section, the hydrophilicity of selected amino acid side chains was found to affect biological activity and membrane selectivity, as evidenced by the code 28 sequence displaying good activity against MRSA, whereas the substitution of lysine with histidine significantly decreased the activity (code 29). Furthermore, the replacement of polar serine (code 30) with negatively charged glutamic acid (code 31) also reduced the activity (Table 1) because of the repulsive electrostatic interaction of negatively charged glutamic acid with the negatively charged cell membrane. On the contrary, an increase in the number of positively charged amino acids, such as lysine, arginine, and histidine, from two to three (codes 32–37; Table 1) resulted in high activity against MRSA. Examples illustrating the alteration of membrane selectivity in a manner dependent on peptide sequences focused on comparing code 38–41 sequences (Table 1). The

code 38 peptide with two consecutive positively charged lysines showed broad-spectrum activity against either gram-positive MRSA or gram-negative *E. coli*, whereas the replacement of one lysine residue with a histidine of the same charge (code 39) led to the persistence of the activity against MRSA but caused a significant decrease of the activity against *E. coli* (Table 1). Moreover, the substitution of a single lysine with a polar serine (code 40) or two consecutive lysines with arginine of the same charge (code 41) in the code 38 peptide sequence (Table 1) resulted in complete inactivation and selective activity against *E. coli*, respectively.

Similar to the antiviral characteristics [50], enantiomeric (codes 43 and 44) and retroenantiomeric (codes 52 and 53) peptide sequences showed similar antibacterial activities, which was also in accordance with the experimental results presented by Fletcher et al. [52] (codes 50 and 51) and Dartois et al. [53] (codes 71 and 72). Fletcher et al. [52] screened a series of hexa cyclic peptides with a positive charge and a large amphiphilic distribution of hydrophobic and hydrophilic residues against bacteria with different cytoplasmic membrane compositions, including MRSA, *E. coli*, *Ulva linza*, and *Navicula perminuta*. Further sequence–activity comparison indicated that the activity and selectivity of peptides against bacteria were largely determined by the degree of amphiphilicity but not by the overall cationic charge [52]. For example, amphiphilic cationic peptides of codes 54 and 55 showed MRSA (gram-positive) selectivity, whereas unique mixed topological cationic peptides of codes 50 and 51 (Table 1) against *E. coli* (Gram-negative) suggested that the histidine residue located in the middle of two hydrophobic amino acids acts as a deprotonated hydrophobic residue. The data of code 50 and codes 56–62 sequences in Table 1 show that the single substitution of an amino acid with hydrophilic lysine, arginine, histidine, and serine residues results in broad-spectrum activity against MRSA, *E. coli*, *U. linza*, and *N. perminuta*, whereas those sequences with hydrophobic tyrosine, tryptophan, and phenylalanine residues generally become inactive [52]. Similar results were also found when comparing the single-substitution peptide sequences of code 54 and codes 63–67, as well as the experimental results of Dartois [53] (codes 71–76; Table 1), who illustrated the importance of preserving hydrophilic lysine, arginine, histidine, and serine residues to design peptides with broad-spectrum antibacterial activity [52].

In addition to nonglycosylated cyclic peptides, cationic cyclic D,L-α-glycopeptides bearing side chain derivatives with D-glucosamine (codes 77–79; Table 1), D-galactose (codes 80 and 81; Table 1), or D-mannose (codes 82 and 83; Table 1) were also demonstrated to self-assemble, form β-sheet-like supramolecular nanotubes, and act against MRSA and vancomycin-resistant *Enterococcus faecalis* with respective MICs of 2.5–5 μM and 10–15 μM (Table 1). These activities were exposed by enhancing membrane permeability, as evidenced in liposome-based fluorescence dye release assays and attenuated total reflectance FT-IR spectroscopy in synthetic membranes [54].

2.3. *Drug delivery*

Owing to their high surface area and the different properties of their hollow core and external surfaces, several studies have demonstrated that either the physical cotreatment of cPNTs with anticancer drugs [55] or their complexation with anticancer drugs with surface modification by polymers [56–58] could reduce the IC_{50} in various cancer cell lines compared with that for the drug alone (Table 2) [55–58]. Chen et al. [55] found that the liposomal membrane release of anticancer drug 5-FU was enhanced by the addition of a highly hydrophobic cyclic peptide, namely, cyclo-[Gln-(D-Leu-Trp)$_4$-D-Leu], in a dose-dependent manner. Furthermore, in BEL7402, HeLa, and S180 cells cotreated with 5-FU and these cPNTs, the cytotoxic effect was enhanced, as evidenced by the decrease in IC_{50} (Table 2). Further mechanistic studies suggested that physical cotreatment with cyclo- [Gln-(D-Leu-Trp)$_4$-D-Leu] does not destroy the cell membrane [55]. The permeation of drugs smaller than the internal diameter of cPNTs, such as 5-FU (0.44 nm), may occur through the hydrophilic channel of cPNTs in a dose-dependent manner [55]. On the basis of conventional MD computation and steered MD simulations, it was proposed that cPNTs hop along cPNT subunits by switching from the hydrophobic interaction between 5-FU and the interior wall of the cPNTs to the hydrogen bonding interactions of 5-FU with backbone carbonyl groups and amide groups of cPNTs [59].

Furthermore, drugs that were conjugated or complexed with differently sized or surface-modified cPNT nanotubes either by peptide sequence alteration or by polymer modification were found to enhance cytotoxicity and could be involved in different mechanisms of action. For example, both PEG-modified doxorubicin-loaded cyclo-(Gln-D-Ala-Glu-D-Ala-Gln-D-Ala-Cys-D-Ala) cPNTs with 10 nm diameter and 50–80 nm length [57] and HEA-co-CEMA-conjugated ruthenium-loaded cyclo-(azido-Lys-D-Leu-Trp-D-Leu)$_2$ with 20 nm diameter and 200–500 nm length [58] showed higher in vitro cellular uptake results with higher cytotoxicity than free drugs in MCF-7 and A2780 cells, respectively (Table 2). Free doxorubicin was mainly located outside the endolysosome, whereas the PEG-modified doxorubicin/cPNT complex was predominantly located in the endolysosome, thus revealing that complex uptake may involve the endocytotic pathway [57]. The high cytotoxicity result obtained after altering the drug distribution among the cell organelles were also observed when iridium-loaded cyclo-(D-Leu-Lys-D-Leu-Trp)$_2$ cPNTs were modified with HPMA-co-PUEMA, which augmented the amount of drug distributed in the membrane fraction from 56% with the drug alone to 69% with the conjugated form; this result illustrates the involvement of the endocytotic mechanism [56]. However, the amount of cellular uptake of drug molecules was not increased, thus suggesting that cPNTs exhibited a more effective mode of action via the different partitioning of the drug in the cell [56]. In addition to in vitro experiments, in vivo results were also obtained. These showed that in mice with S180 tumors that were intratumorally injected with a physical combination of 5-FU and 0.25 mg cPNTs per kilogram body weight, these molecules had synergistic effects on tumor size, with a significant reduction of 46.6% in volume and 61.9% in weight compared with those treated with 5-FU alone [55]. In accordance with this result, further tissue section observations revealed that the necrosis and shrinkage of tumor cells were

Table 2 – Cyclic peptide nanotubes (cPNTs) as drug and gene delivery vectors.

Cyclic Peptide Sequence	Conjugate Polymer	Drug	Tube Size (μm)	Drug Delivery							Reference
				IC_{50} (μM)							
				A2780	A2780cis	MCF-7	MCF-7/ADR	BEL7402	HeLa	S180	
None	None	5-Fluorouracil	ND	ND	ND	ND	ND	596	1460	1790	[55]
Gln-(D-Leu-Trp)$_4$-D-Leu	None	5-Fluorouracil	ND	ND	ND	ND	ND	241	819	389	
None	None	Doxorubicin	ND	ND	ND	0.53 ± 0.05	4.21 ± 0.65	ND	ND	ND	[57]
Gln-D-Ala-Glu-D-Ala-Gln-D-Ala-Cys-D-Ala	PEG	Doxorubicin	Length: 0.05–0.08 Width: 0.01	ND	ND	0.16 ± 0.03	0.84 ± 0.04	ND	ND	ND	
None	None	Ruthenium	ND	271	266	ND	ND	ND	ND	ND	[58]
(Azido-Lys-D-Leu-Trp-D-Leu)$_2$	HEA-co-CEMA	Ruthenium	Length: 0.2–0.5	15	22	ND	ND	ND	ND	ND	
None	None	Iridium	ND	0.95 ± 0.03	ND	ND	ND	ND	ND	ND	[56]
None	HPMA-co-PUEMA	Iridium	ND	1.80 ± 0.09	ND	ND	ND	ND	ND	ND	
(D-Leu-Lys-D-Leu-Trp)$_2$	HPMA-co-PUEMA	Iridium	Length: 0.022 ± 0.001	0.61 ± 0.02	ND	ND	ND	ND	ND	ND	

Cyclic Peptide Sequence	Conjugate Polymer	Gene	Tube Size (μm)	Gene Delivery				Reference
				Cell	Aimal	Route	Expression Organ	
(D-Ala-Lys)$_4$	None	pF143-GFP	Width: 0.01–0.4	HeLa HEK-293	None	None	None	[60]
D-Trp-Tyr	None	pCMV-*LacZ*	Length: 1-20	None	Mice	Oral	Stomach Duodeum	[32]
		pCMV-*hRluc*	Width: 0.1–0.8				Liver Kidney	
D-Trp-Tyr	None	pCMV-bcl-$_{xL}$-eGFP CAP3 pRFP-C-RS	Length: 1.4 ± 0.8 Width: 0.26 ± 0.06	None	Mice	Eye	Cornea	[61]

IC_{50}: half-inhibition concentration; HPMA: Hydroxypropyl methacrylamide; PUEMA: 2-(3-(Pyridin-4-ylmethyl)ureido)ethyl)methacrylate; HEA: 2-Hydroxyethyl acrylate; CEMA: 2-Chloroethyl methacrylate; ND: Non-detected;

accompanied by waxed intracellular space, condensed nucleus, and newly emerged vacuoles; these findings indicate that the antitumor effect of 5-FU was intensified by cPNTs [55].

2.4. Gene delivery

Cyclic octa- and di-cPNTs have been revealed to function as gene delivery vectors [32,60,61]. For example, cyclic octa-cPNTs with widths of 10–400 nm and lengths of micrometers composed of four L-lysines and four D-alanines with one lysine residue functionalized by a guanidiniocarbonyl pyrrole moiety were found to be able to interact with negatively charged calf thymus DNA via positively charged lysine residues that formed aggregates; their results show that cyclic octa-cPNTs may be able to deliver genes into cells without the involvement of the endocytotic pathway [60]. The transfection results after incubation with HeLa cells for 24 h revealed that the DNA–cPNT complex was comparable with the positive controlled PEI group but with less cytotoxicity than PEI (Table 2) [60]. Cyclo-(D-Trp-Tyr) cPNTs with widths of 100–800 nm and lengths of 1–20 μm were also proven to successfully deliver plasmid DNA by oral administration in vivo in an energy-dependent manner [32]. DNA was found to interact with tyrosine residues of cyclo-(D-Trp-Tyr) cPNTs with a binding constant of $3.2 \times 10^8\ M^{-1}$ [32]. The delivery of these cPNTs with either pCMV-*LacZ* or pCMV-*hRluc* plasmids by oral administration respectively showed β-Gal or Renilla luciferase protein expression in the chief cells; parietal cells; fundus glands; gastric pits; the mucosa surface epithelium of the stomach, crypt cells, and lamina propria; and the villous epithelium of duodenal villi, lobules, hepatocytes and sinusoidal endothelial cells near the portal vein of the liver, endothelial cells of proximal tubular, and endothelial cells of the glomerulus of the renal cortex (Table 2) [32]. The successful protein expression may have resulted from the enhancement of stability at an acidic pH for 60 min, in bile for 180 min, and in the presence of enzymes for 50 min; it may also have involved the enhancement of permeability from $49.2 \pm 21.6 \times 10^{-10}$ cm/s for naked DNA to $395.6 \pm 142.2 \times 10^{-10}$ cm/s for DNA/cPNT complexes in the gastrointestinal tract, which involved an energy-dependent pathway and the sustained release of DNA from 5.92×10^{11} copies of DNA/$t^{1/2}$ for naked DNA to 3.57×10^{11} copies of DNA/$t^{1/2}$ for the cPNT formulated DNA [32]. Furthermore, the eye drops delivery of plasmid-encoded caspase 3 silencing shRNA and CAP3 pRFP-C-RS with cyclo-(D-Trp-Tyr) cPNTs with an average width of 290 nm and length of 1.8 μm in a corneal epithelial debridement model also revealed the ability to significantly decrease the caspase 3 activity (Table 2) [61].

2.5. Organic electronics

In recent years, organic electronics has been studied as an alternative to silicon electronics because of the advantage of high designability. Conjugated polymers on the surface of conducting materials are one aspect of organic electronics. For example, by using a current-sensing AFM (CS-AFM) with a conducting Pt/Ir cantilever on a gold mica substrate, Uji et al. [62] tested the electric properties of cPNTs with lengths of more than 100 μm and widths of several microns stacked by cyclo-$(Ala)_3$ with tetrathiafulvalene as a side chain. The results indicated that cyclo-$(Ala)_3$ with the tetrathiafulvalene modification exhibited p-type semiconductor properties (Table 3) [62]. Further detailed evaluations of the current fluctuation revealed that these cPNTs acted as dielectric materials in a manner that is dependent on the applied potential. Lee et al. [63] discovered that cyclo-(Phe–Phe) nanotubes made by vapor-phase self-assembly also exhibited semiconductor properties (Table 3). Specifically, the current increased with increasing temperature from 273 to 387 K under a steady voltage [63]. These findings illustrate that cPNTs have potential as materials for organic electronics in the fabrication of nanoelectronic sensors for the ultrasensitive detection of protein and viral particles, as well as for the recording, stimulation, and inhibition of neuronal signals in nanowire–neuron hybrid structures [64].

2.6. Channels

Channels that cross lipid bilayer membranes play a role in the selective and efficient transport of ions or molecules and are essential for cell viability. In the last decade, researchers have attempted to develop artificial ion channels by using simple molecules that possess self-assembly properties. Cyclic D,L-α-peptides [65–80], cyclic β-peptides [81], and cyclic α-γ-peptides [82] that were found to be able to self-assemble as transmembrane cPNTs were considered to have potential as artificial channels for ionic and molecular transport (Table 3) [65]. Different ions and molecules exhibit different transportation behaviors and mechanisms depending on the radius [66–69], length [70], and surface properties (hydration ability and charge) of cPNTs [65,71], as well as on the strength of the electric field [72,73], the open-ended orientation of cPNTs on the membrane surface [74], the concentration of ions or molecules [65,82], the size of the molecules, and the temperature [72]. Generally, the determination of the free energy or diffusion coefficient is a conventional approach used to clarify the feasibility of ionic or molecular transport via cPNTs. The transportation of cations, including K^+ [66,72,75,76], Na^+ [66,72,75–77], Ca^{2+} [66], and NH_4^+ [67], in cPNTs constructed using different types and numbers of peptides have been studied by MD simulations (Table 3). Among these cations, K^+ and Na^+ revealed similar low-energy barriers and diffusion coefficients, thus indicating the easy transport of these two ions in cyclo-(D-Ala-Glu-D-Ala-Gln)$_2$ [75] and cyclo-(Trp-D-Leu)$_{n=4,5}$ cPNTs [66,76,77]. By contrast, Ca^{2+} was calculated to have a higher energy barrier than K^+ and Na^+; therefore, it was considered that it did not easily enter cyclo-(Trp-D-Leu)$_4$ cPNTs but may enter cyclo-(Trp-D-Leu)$_5$ cPNTs with large radii [66]. Different cations may also be involved in different modes of interaction within cPNTs. Calcium ions and sodium ions were proposed to interact with the framework of octa-cPNTs predominantly via water bridge interaction [66,75]. The electrostatic interaction of calcium and sodium ions with water molecules resulted in a densely packed distribution of channel water around these cations, thus forming a stable solvation structure in cPNTs that reduced the diffusion. On the contrary, the incomplete solvation of potassium ions with

Table 3 – Cyclic peptide nanotubes (cPNTs) for organic electronic and molecular channels.

Cyclic Peptide Sequence	Side Chain Modification	Organic Electronic		Reference
		Size (μm)	Current–Voltage Curve	
$(\beta\text{-Ala})_3$	Tetrathiafulvalene	(L): >100 (W): several μm	P-Type SemiconductorJunction	[62]
Phe–Phe	None	(L): >10 (W): 0.09	Symmetrical Temperature-Dependent Characteristic (Schottky-like barrier)	[63]

Cyclic Peptide Sequence	Membrane Lipid	Diameter (Å)	Length (Å)	Ion Channels						Reference
				Model	Transport Ions/ Molecules	Applied Voltage (mV)	Transport Rate	Diffusion Coefficient (m^2/sec)	Free Energy (kcal/mol)	
$(\text{D-Ala-Glu-D-Ala-Gln})_2$	None	4.87	ND	PMF	Na^+	None	ND	$0.5–1 \times 10^{-9}$	2.4	[75]
					K^+			$0.5–1 \times 10^{-9}$	2.4	
$(\text{Trp-D-Leu})_4$	DMPC	6.25	70	Position Dependent	Na^+	None	ND	0.0141×10^{-9}	ND	[76]
					K^+			0.0203×10^{-9}	ND	
$(\text{Trp-D-Leu})_4$	POPE	5	26	PMF	Na^+	None	ND	ND	3.5	[77]
	POPE	5	26	vdW interaction energies	Na^+	None	ND	ND	0 (Na^+-cPNT) 12 (Na + -water) 0 (Na^+–POPE)	
	POPE	5	26	Electrostatic	Na^+	None	ND	ND	−35~−70 (Na^+-cPNT) −120~−165 (Na^+-water) 15~−5 (Na^+–POPE)	
$(\text{Trp-D-Leu})_4$	POPE	4.6	33.6	PMF	Ca^{2+}	None	ND	ND	35	[66]
					Na^+				3.5	
					K^+				3.4	
$(\text{Trp-D-Leu})_5$	POPE	5.8	33.6		Ca^{2+}	None	ND	ND	10	
					Na^+				3.5	
					K^+				3	
$(\text{D-Ala-Gln-D-Ala-Glu})_3$	None	13	37	TIP3P	Na^+	100	ND	0.0001×10^{-9}	ND	[72]
						200	ND	0.0007×10^{-9}	ND	
						300	ND	0.0183×10^{-9}	ND	
						400	ND	0.0526×10^{-9}	ND	
						500	ND	0.0895×10^{-9}	ND	
	None	13	37	TIP3P	K^+	100	ND	ND	ND	
						200	ND	0.0009×10^{-9}	ND	
						300	ND	0.0016×10^{-9}	ND	
						400	ND	0.0205×10^{-9}	ND	
						500	ND	0.0699×10^{-9}	ND	

(continued on next page)

Table 3 – (*continued*)

Cyclic Peptide Sequence	Membrane Lipid	Diameter (Å)	Length (Å)	Ion Channels						Reference
				Model	Transport Ions/ Molecules	Applied Voltage (mV)	Transport Rate	Diffusion Coefficient (m^2/sec)	Free Energy (kcal/mol)	
$(Trp\text{-}D\text{-}Leu)_4$	POPE	4.8	ND	PMF	NH_3 NH_4^+	None	ND	ND	0.8–1.6 1–4	[67]
$(Trp\text{-}D\text{-}Leu)_5$	POPE	5.8	ND	PMF	NH_3 NH_4^+	None	ND	ND	1–2.2 0.3–2.5	
$(Trp\text{-}D\text{-}Leu)_4$	POPE	4.8	ND	vdW interaction energies	NH_3,NH_4^+	None	ND	ND	0~–2.5 (NH_3-cPNT) 0–4 (NH_3-water) 0(NH_4^+-cPNT) 10 (NH_4^+-water)	
$(Trp\text{-}D\text{-}Leu)_5$	POPE	5.8	ND	vdW interaction energies	NH_3,NH_4^+	None	ND	ND	0~–2 (NH_3-cPNT) 3–5 (NH_3-water) 0(NH_4^+-cPNT) 10 (NH_4^+-water)	
$(Trp\text{-}D\text{-}Leu)_4$	POPE	4.8	ND	Electrostatic	NH_3,NH_4^+	None	ND	ND	0~–2.5 (NH_3-cPNT) –13 (NH_3-water) –10~–60 (NH_4^+-cPNT) –110 (NH_4^+-water)	[67]
$(Trp\text{-}D\text{-}Leu)_5$	POPE	4.8	ND	Electrostatic	NH_3,NH_4^+	None	ND	ND	0~–2 (NH_3-cPNT) –20 (NH_3-water) –10~–50 (NH_4^+-cPNT) –120 (NH_4^+-water)	
$(Trp\text{-}D\text{-}Leu)_3$	POPE	6.8	33.5	Equilibrium MD Simulation	H_2O	None	0.12 (ns^{-1})	$0.055 \pm 0.005 \times 10^{-9}$	0.35	[68]
$(Trp\text{-}D\text{-}Leu)_4$		8.2					1.53 ± 0.23 (ns^{-1})	$0.62 \pm 0.08 \times 10^{-9}$	0.28	
$(Trp\text{-}D\text{-}Leu)_5$		10.6					25.2 (ns^{-1})	$1.3 \pm 0.15 \times 10^{-9}$	0.25	
$(Trp\text{-}D\text{-}Leu)_4$	POPE	8	24	Equilibrium MD Simulation	H_2O	None	1.53 ± 0.23 (ns^{-1})	$0.467 \pm 0.069 \times 10^{-9}$	ND	[70]
	POPE	8	28.8	Equilibrium MD Simulation	H_2O	None	1.27 ± 0.21 (ns^{-1})	$0.386 \pm 0.063 \times 10^{-9}$	ND	
	POPE	8	33.6	Equilibrium MD Simulation	H_2O	None	0.89 ± 0.14 (ns^{-1})	$0.271 \pm 0.043 \times 10^{-9}$	–17~–19 (H_2O-cPNT) 0 (H_2O–H_2O) –2~–7(H_2O-POPE)	
	POPE	8	38.4	Equilibrium MD Simulation	H_2O	None	0.83 ± 0.17 (ns^{-1})	$0.234 \pm 0.049 \times 10^{-9}$	ND	
	POPE	8	43.2	Equilibrium MD Simulation	H_2O	None	0.53 ± 0.13 (ns^{-1})	$0.163 \pm 0.041 \times 10^{-9}$	–17~–20 (H_2O-cPNT) 0 (H_2O–H_2O) –2~–7(H_2O-POPE)	
$(Trp\text{-}D\text{-}Leu)_4$	POPE	8	33.6	TIP3P	H2O	0	393.0 ± 4.5 (ns^{-1})	ND	0~–25 (H_2O-cPNT) 50~–70 (H_2O–H_2O) 30~–70 (Total)	[73]
	POPE	8	33.6	TIP3P	H2O	100	384.1 ± 4.4 (ns^{-1})	ND	0~–30 (H_2O-cPNT) 50~–80 (H_2O–H_2O) 50~–100 (Total)	
	POPE	8	33.6	TIP3P	H2O	300	378.3 ± 4.3 (ns^{-1})	ND	20~–30 (H_2O-cPNT) 100~–80 (H_2O–H_2O) 80~–120 (Total)	

$(Trp\text{-}D\text{-}Leu)_4$	POPE	8	33.6	TIP3P	H2O	500	353.5 ± 4.2 (ns^{-1})	ND	20~−30 (H_2O-cPNT) 100~−80 (H_2O−H_2O) 90~−120 (Total)	[73]
	POPE	8	33.6	TIP3P	H2O	700	293.1 ± 3.8 (ns^{-1})	ND	20~−30 (H_2O-cPNT) 100~−80 (H_2O−H_2O) 95~−120 (Total)	
	POPE	8	33.6	TIP3P	H2O	900	257.2 ± 3.6 (ns^{-1})	ND	20~−30 (H_2O-cPNT) 100~−80 (H_2O−H_2O) 100~−120 (Total)	
$(Trp\text{-}D\text{-}Leu)_4$	POPE	8	33.6	PMF	O_2 CO_2 NH_3	None	ND	ND	0.5−1.5 0.2−1 0.2−1.2	[79]
	POPE	8	33.6	vdW interaction energies	O_2	None	ND	ND	−3.8~−4.2 (O_2-cPNT) −0.2~−0.6 (O_2−H_2O)	
	POPE	8	33.6	vdW interaction energies	CO_2	None	ND	ND	−5.8~−6.2 (CO_2-cPNT) −0.2~−1 (CO_2−H_2O)	
	POPE	8	33.6	vdW interaction energies	NH_3	None	ND	ND	−2.5 (NH_3-cPNT) 2.5−4 (NH_3−H_2O)	
$(Trp\text{-}D\text{-}Leu)_4$	POPE	8	33.6	Electrostatic	O_2	None	ND	ND	0 (O_2-cPNT) 0 (O_2−H_2O)	[79]
	POPE	8	33.6	Electrostatic	CO_2	None	ND	ND	−0.2~−0.6 (CO_2-cPNT) −0.4~−1 (CO_2−H_2O)	
	POPE	8	33.6	Electrostatic	NH_3	None	ND	ND	−0.2−0.2 (NH_3-cPNT) −12~−18 (NH_3−H_2O)	
$(Trp\text{-}D\text{-}Leu)_4$	POPE	8	33.6	PMF	Methane Methanol Ethanol	None	ND	ND 0.27 (Methanol/H_2O = 0.2) 0.09 (Ethanol/H_2O = 0.2)	7 4.5 6.3	[71]
	POPE	8	33.6	vdW interaction energies	Methane	None	ND	ND	−5.5 (Methane-cPNT) −0.1~−1 (Methane-H_2O)	
	POPE	8	33.6	vdW interaction energies	Methanol	None	ND	ND	−7.5 (Methaol-cPNT) 1−2 (Methanol-H_2O)	
	POPE	8	33.6	vdW interaction energies	Ethanol	None	ND	ND	−8~−12 (Ethanol-cPNT) 0−1.5 (Ethanol-H_2O)	
$(Trp\text{-}D\text{-}Leu)_4$	POPE	8	33.6	Electrostatic	Methane	None	ND	ND	0 (Methane-cPNT) 0~−0.2 (Methane-H_2O)	[71]
	POPE	8	33.6	Electrostatic	Methanol	None	ND	ND	−1.5 (Methaol-cPNT) −7~−12 (Methanol-H_2O)	
	POPE	8	33.6	Electrostatic	Ethanol	None	ND	ND	−1.5~−2.5 (Ethanol-cPNT) −4~-10 (Ethanol-H_2O)	
$(Trp\text{-}D\text{-}Leu)_3$ $(Trp\text{-}D\text{-}Leu)_4$ $(Trp\text{-}D\text{-}Leu)_5$	POPE	6 8 10	33.6	PMF	Ethaol	None	ND	None 2.3×10^{-15} 5.53×10^{-15}	None 0.6−4.8 0.5−2	[78]
$(Trp\text{-}D\text{-}Leu)_4$	POPE	8	33.6	vdW interaction energies	Ethaol	None	ND	ND	−9 (Ethanol-cPNT) −1 (Ethanol−Ethanol)	
$(Trp\text{-}D\text{-}Leu)_5$	POPE	10	33.6	vdW interaction energies	Ethaol	None	ND	ND	−6 (Ethanol-cPNT) 0~−2 (Ethanol−Ethanol)	

(continued on next page)

Table 3 – (continued)

Cyclic Peptide Sequence	Membrane Lipid	Diameter (Å)	Length (Å)	Ion Channels						Reference
				Model	Transport Ions/ Molecules	Applied Voltage (mV)	Transport Rate	Diffusion Coefficient (m^2/sec)	Free Energy (kcal/mol)	
$(Trp\text{-}D\text{-}Leu)_4$	POPE	8	33.6	Electrostatic	Ethaol	None	ND	ND	−2~−5 (Ethanol-cPNT) −4~−6 (Ethanol−Ethanol)	[78]
$(Trp\text{-}D\text{-}Leu)_5$	POPE	10	33.6	Electrostatic	Ethaol	None	ND	ND	−1~−11 (Ethanol-cPNT) −7.5~−15 (Ethanol−Ethanol)	

TIP3P: Transferable intermolecular potential water molecule model; DMPC: 1,2-Dimyristoyl-sn-glycero-3-phosphocholine; POPE: 1-palmitoyl-2-oleoyl-sn-glycero-3-phosphoethanolamine; PMF: Potential of mean force; ND: Non-detected. (L): length; (W): width.

water led to the direct coordination of unstable potassium ions with the carbonyl oxygen of octa-cPNTs [66,75]. NH_4^+ with a high energy barrier as a result of more electrostatic interaction and water bridge hydrogen bonding was shown to be trapped at the α-plane zone in cyclo-$(Trp\text{-}D\text{-}Leu)_4$ cPNTs [67].

In addition to ions, the transportation of molecules including water [65,68,70,73], O_2 [79], CO_2 [79], NH_3 [79], methane [71], methanol [65,71], ethanol [71,78], and chloroform [65] within cPNTs was also evaluated by MD simulations (Table 3). Water molecules exhibit different permeation properties in cPNTs with an altered radius and length (Table 3) [68,70]. Generally, the larger radius of cPNTs facilitates water diffusion, as evidenced by the results of Liu [68], who showed that the diffusion coefficients of water molecules in hexa-, octa-, and deca-cyclo-(Trp-D-Leu) cPNTs were $0.055 \pm 0.005 \times 10^{-9}$, $0.62 \pm 0.08 \times 10^{-9}$, and $1.3 \pm 0.15 \times 10^{-9}$ m^2/s, respectively; these findings were positively related to radius size [68]. By contrast, the osmotic permeability (Pf) of water in cyclo-$(Trp\text{-}D\text{-}Leu)_4$ cPNTs was found to decrease with the increasing length of the channel, thus indicating the relatively rapid transport in short channels [70]. Water molecules were found to be distributed in channels in a single file, in a 1-2-1-2 wavelike formation, and in completely chaotic patterns within hexa-, octa-, and deca-cyclo-(Trp-D-Leu) nanotubes [68]. In cyclo-$(Trp\text{-}D\text{-}Leu)_4$ cPNTs, two water molecules were considered to be located in the midplane zone forming a hydrogen bond with one adjacent water molecule distributed in the α-plane zone and forming a water chain inside the channel [80]. Water molecules near the ends of the two cPNTs were further clarified to have strong orientating forces in opposite directions that point to the cPNT center [80]. By contrast, the orientating force of water molecules in the center of cPNTs was shown to be relatively weak [80]. Under a gradient electric field that increased from 0.3 to 0.9 V/nm, water molecules in the axial orientation became more compact as a result of enhancing the hydrogen-bonded network of the channel water (Table 3) [73]. By comparing the transport properties of gas molecules O_2, CO_2, and NH_3, different external forces were shown to be needed for these gas molecules to enter cyclo-$(Trp\text{-}D\text{-}Leu)_4$ cPNTs (Table 3). The transport of these three gas molecules involved direct and water-bridged hydrogen bond interactions [79]. NH_3 molecules were found to more easily generate hydrogen bonds with water molecules in the channel, thus forming single or double water bridges and leading to a lower external force needed to transport NH_3 than for O_2 and CO_2 molecules [79]. Larger molecules such as methane, methanol, and ethanol were also considered to have difficulty passing through cyclo-$(Trp\text{-}D\text{-}Leu)_4$ cPNTs because of their high energy barrier [71], which may be overcome by the application of cPNTs with larger radii [78]. Overall, these results illustrate the promise of using cPNTs for artificial channels for the selective or nonselective transport of ions or molecules.

3. Final remarks

This mini-review reveals the versatility of cPNTs for a range of applications in the biomedical field. Although the development of cPNTs has generated increasing interest, some issues

need to be analyzed and overcome. Safety is the most important issue for any material for biomedical use. Although many studies have proved the safety of cPNTs in vitro, more in vivo studies are necessary for further critical analyses. Furthermore, size control plays an important role in the successful delivery of active pharmaceutical ingredients via nanodevices. To date, there have been few discussions on the manufacturing methods for controlling the uniformity of PNTs, particularly regarding length and bundle width. Nonetheless, the versatility and tunability of these structures should drive the development of more ingenious applications of cPNTs in the biomedical field.

Funding

This work was supported by grants from the Ministry of Science and Technology, Taiwan [MOST 107-2320-B-038 -045 and MOST 107-2321-B-006 -016].

Conflicts of interest

The authors declare no competing financial interest.

REFERENCES

[1] Wilczewska AZ1, Niemirowicz K, Markiewicz KH, Car H. Nanoparticles as drug delivery systems. Pharmacol Rep 2012;64:1020–37.
[2] Caldorera-Moore M, Guimard N, Shi L, Roy K. Designer nanoparticles: incorporating size, shape and triggered release into nanoscale drug carriers. Expet Opin Drug Deliv 2010;7:479–95.
[3] Blanco E, Shen H, Ferrari M. Principles of nanoparticle design for overcoming biological barriers to drug delivery. Nat Biotechnol 2015;33:941–51.
[4] Kulkarni SA, Feng SS. Effects of particle size and surface modification on cellular uptake and biodistribution of polymeric nanoparticles for drug delivery. Pharm Res (N Y) 2013;30:2512–22.
[5] Geng Y, Dalhaimer P, Cai S, Tsai R, Tewari M, Minko T, et al. Shape effects of filaments versus spherical particles in flow and drug delivery. Nat Nanotechnol 2007;2:249–55.
[6] Nishiyama N. Nanomedicine: nanocarriers shape up for long life. Nat Nanotechnol 2007;2:203–4.
[7] Simone EA, Dziubla TD, Muzykantov VR. Polymeric carriers: role of geometry in drug delivery. Expet Opin Drug Deliv 2008;5:1283–300.
[8] Bruckman MA, Randolph LN, VanMeter A, Hern S, Shoffstall AJ, Taurog RE, et al. Biodistribution, pharmacokinetics, and blood compatibility of native and PEGylated tobacco mosaic virus nano-rods and -spheres in mice. Virology 2014;449:163–73.
[9] Gratton SE, Ropp PA, Pohlhaus PD, Luft JC, Madden VJ, Napier ME, et al. The effect of particle design on cellular internalization pathways. Proc Natl Acad Sci U S A 2008;105:11613–8.
[10] Jogi H, Maheshwari R, Raval N, Kuche K, Tambe V, Mak KK, et al. Carbon nanotubes in the delivery of anticancer herbal drugs. Nanomedicine 2018;15:1187–220.
[11] Pantarotto D, Briand JP, Prato M, Bianco A. Translocation of bioactive peptides across cell membranes by carbon nanotubes. Chem Commun 2004;1:16–7.
[12] Kam NWS, Jessop TC, Wender PA, Dai H. Nanotube molecular transporters: internalization of carbon nanotube-protein conjugates into mammalian cells. J Am Chem Soc 2004;126:6850–1.
[13] Riley II MK, Vermerris W. Recent advances in nanomaterials for gene delivery-A review. Nanomaterials 2017;7:94.
[14] Wang L, Shi J, Zhang H, Li H, Gao Y, Wang Z, et al. Synergisticanticancer effect of RNAi and photothermal therapy mediated by functionalized single-walled carbon nanotubes. Biomaterials 2013;34:262–74.
[15] Chen X, Klingeler R, Kath M, Gendy AAEl, Cendrowski K, Kalenczuk RJ, et al. Magnetic silica nanotubes: synthesis, drug release, and feasibility for magnetic hyperthermia. ACS Appl Mater Interfaces 2012;4:2303–9.
[16] Ilbasmis-Tamer S, Unsal H, Tugcu-Demiroz F, Kalaycioglu GD, Degim IT, Aydogan N. Stimuli-responsive lipid nanotubes in gel formulations for the delivery of doxorubicin. Colloids Surfaces B Biointerfaces 2016;143:406–14.
[17] Bilal T, Gözen I. Formation and dynamics of endoplasmic reticulum-like lipid nanotube networks. Biomater Sci 2017;5:1256–64.
[18] Komatsu T. Protein-based nanotubes for biomedical applications. Nanoscale 2012;4:1910–8.
[19] Qu X, Komatsu T. Molecular capture in protein nanotubes. ACS Nano 2010;4:563–73.
[20] Silva RF, Araújo DR, Silva ER, Ando RA, Alves WA. L-diphenylalanine microtubes as a potential drug-delivery system: characterization, release kinetics, and cytotoxicity. Langmuir 2013;29:10205–12.
[21] Wang J, Liu G, Jan MR. Ultrasensitive electrical biosensing of proteins and DNA: carbon-nanotube derived amplification of the recognition and transduction events. J Am Chem Soc 2004;126:3010–1.
[22] Boussaad S, Tao NJ, Zhang R, Hopson T, Nagahara LA. In situ detection of cytochrome c adsorption with single walled carbon nanotube device. Chem Commun 2003:1502–3.
[23] Star A, Gabriel JCP, Bradley K, Gruner G. Electronic detection of specific protein binding using nanotube FET devices. Nano Lett 2003;3:459–63.
[24] Azamian BR, Davis JJ, Coleman KS, Bagshaw CB, Green MLH. Bioelectrochemical single-walled carbon nanotubes. J Am Chem Soc 2002;124:12664–5.
[25] Poland CA, Duffin R, Kinloch I, Maynard A, Wallace WA, Seaton A, et al. Carbon nanotubes introduced into the abdominal cavity of mice show asbestoslike pathogenicity in a pilot study. Nat Nanotechnol 2008;3:423–8.
[26] Lam C-W, James JT, McCluskey R, Hunter RL. Pulmonary toxicity of single-walled carbon nanotubes in mice 7 and 90 days after intratracheal instillation. Toxicol Sci 2004;77:126–34.
[27] Muller J, Huaux F, Moreau N, Misson P, Heilier JF, Delos M, et al. Respiratory toxicity of multi-wall carbon nanotubes. Toxicol Appl Pharmacol 2005;207:221–31.
[28] Carrero-Sanchez JC, Elias AL, Mancilla R, Arrellin G, Terrones H, Laclette JP, et al. Biocompatibility and toxicological studies of carbon nanotubes doped with nitrogen. Nano Lett 2006;6:1609–16.
[29] Silk DB, Grimble GK, Rees RG. Protein digestion and amino acid and peptide absorption. Proc Nutr Soc 1985;44:63–72.
[30] Seabra AB, Durán N. Biological applications of peptides nanotubes: an overview. Peptides 2013;39:47–54.
[31] Zohrabi T, Habibi N, Zarrabi A, Fanaei M, Lee LY. Diphenylalanine peptide nanotubes self-assembled on

functionalized metal surfaces for potential application in drug-eluting stent. J Biomed Mater Res A 2016;104:2280–90.
[32] Hsieh WH, Chang SF, Chen HM, Chen JH, Liaw J. Oral gene delivery with cyclo-(D-Trp-Tyr) peptide nanotubes. Mol Pharm 2012;9:1231–49.
[33] Yang Y, Khoe U, Wang X, Horii A, Yokoi H, Zhang S. Designer self-assembling peptide nanomaterials. Nano Today 2009;4:193–210.
[34] Hamley IW. Peptide nanotubes. Angew Chem Int Ed 2014;53:6866–81.
[35] Gao BX, Matsui H. Peptide-based nanotubes and their applications in bionanotechnology. Adv Mater 2005;17:2037–50.
[36] Chapman R, Danial M, Koh ML, Jolliffe KA, Perrier S. Design and properties of functional nanotubes from the self-assembly of cyclic peptide templates. Chem Soc Rev 2012;41:6023–41.
[37] Donaldson K, Borm PJ, Castranova V, Gulumian M. The limits in testing particle-mediated oxidative stress in vitro in predicting diverse pathologies; relevance for testing of nanoparticles. Part Fibre Toxicol 2009;6:13–20.
[38] Ghadiri MR, Granja JR, Milligan RA, McRee DE, Khazanovich N. Self-assembling organic nanotubes based on a cyclic peptide architecture. Nature 1993;366:324–7.
[39] Seebach d, Matthews JL, Meden A, Wessels T, Baerlocher C, McCusker LB. Cyclo-β-peptides: structure and tubular stacking of cyclic tetramers of 3-aminobutanoic acid as determined from powder diffraction data. Helv Chim Acta 1997;80:173–82.
[40] Amorín M, Castedo L, Granja JR. New cyclic peptide assemblies with hydrophobic cavities: the structural and thermodynamic basis of a new class of peptide nanotubes. J Am Chem Soc 2003;125:2844–5.
[41] Nielsen DS, Shepherd NE, Xu W, Lucke AJ, Stoermer MJ, Fairlie DP. Orally absorbed cyclic peptides. Chem Rev 2017;117:8094–128.
[42] Räder AFB, Reichart F, Weinmüller M, Kessler H. Improving oral bioavailability of cyclic peptides by N-methylation. Bioorg Med Chem 2018;26:2766–73.
[43] Samanen J, Ali F, Romoff T, Calvo R, Sorenson E, Vasko J, et al. Development of a small RGD peptide fibrinogen receptor antagonist with potent antiaggregatory activity *in vitro*. J Med Chem 1991;34:3114–25.
[44] Biron E, Chatterjee J, Ovadia O, Langenegger D, Brueggen J, Hoyer D, et al. Improving oral bioavailability of peptides by multiple N-methylation: somatostatin analogues. Angew Chem Int Ed 2008;47:2595–9.
[45] Yu J, Butelman ER, Woods JH, Chait BT, Kreek MJ. Dynorphin A (1–8) analog, E-2078, is stable in human and rhesus monkey blood. J Pharmacol Exp Therapeut 1997;280:1147–51.
[46] Ahmed F, Pakunlu RI, Srinivas G, Brannan A, Bates F, Klein ML, et al. Shrinkage of a rapidly growing tumor by drug-loaded polymersomes: pH-triggered release through copolymer degradation. Mol Pharmacol 2006;3:340–50.
[47] Fernandez-Lopez S, Kim HS, Choi EC, Delgado M, Granja JR, Khasanov A, et al. Antibacterial agents based on the cyclic D, L-alpha-peptide architecture. Nature 2001;412:452–5.
[48] Lopez CF, Nielsen SO, Ensing B, Moore PB, Klein ML. Structure and dynamics of model pore insertion into a membrane. Biophys J 2005;88:3083–94.
[49] Shi W, Wang J, Fan X, Gao H. Size and shape effects on diffusion and absorption of colloidal particles near a partially absorbing sphere: implications for uptake of nanoparticles in animal cells. Phys Rev E – Stat Nonlinear Soft Matter Phys 2008;78:061914.
[50] Horne WS, Wiethoff CM, Cui C, Wilcoxen KM, Amorin M, Ghadiri MR, et al. Antiviral cyclic D, L-alpha-peptides: targeting a general biochemical pathway in virus infections. Bioorg Med Chem 2005;13:5145–53.
[51] Montero A, Gastaminza P, Law M, Cheng G, Chisari FV, Ghadiri MR. Self-assembling peptide nanotubes with antiviral activity against hepatitis C virus. Chem Biol 2011;18:1453–62.
[52] Fletcher JT, Finlay JA, Callow ME, Callow JA, Ghadiri MR. A combinatorial approach to the discovery of biocidal six-residue cyclic D,L-alpha-peptides against the bacteria methicillin-resistant Staphylococcus aureus (MRSA) and *E. coli* and the biofouling algae Ulva linza and Navicula perminuta. Chemistry 2007;13:4008–13.
[53] Dartois V, Sanchez-Quesada J, Cabezas E, Chi E, Dubbelde C, Dunn C, et al. Systemic antibacterial activity of novel synthetic cyclic peptides. Antimicrob Agents Chemother 2005;49:3302–10.
[54] Motiei L, Rahimipour S, Thayer DA, Wong CH, Ghadiri MR. Antibacterial cyclic D,L-alpha-glycopeptides. Chem Commun 2009;25:3693–5.
[55] Chen J, Zhang B, Xia F, Xie Y, Jiang S, Su R, et al. Transmembrane delivery of anticancer drugs through self-assembly of cyclic peptide nanotubes. Nanoscale 2016;8:7127–36.
[56] Larnaudie SC, Brendel JC, Romero-Canelón I, Sanchez-Cano C, Catrouillet S, Sanchis J, et al. Cyclic peptide-polymer nanotubes as efficient and highly potent drug delivery systems for organometallic anticancer complexes. Biomacromolecules 2018;19:239–47.
[57] Wang Y, Yi S, Sun L, Huang Y, Lenaghan SC, Zhang M. Doxorubicin-loaded cyclic peptide nanotube bundles overcome chemoresistance in breast cancer cells. J Biomed Nanotechnol 2014;10:445–54.
[58] Blunden BM, Chapman R, Danial M, Lu H, Jolliffe KA, Perrier S, et al. Drug conjugation to cyclic peptide-polymer self-assembling nanotubes. Chemistry 2014;20:12745–9.
[59] Liu H, Chen J, Shen Q, Fu W, Wu W. Molecular insights on the cyclic peptide nanotube-mediated transportation of antitumor drug 5-fluorouracil. Mol Pharm 2010;7:1985–94.
[60] Li M, Ehlers M, Schlesiger S, Zellermann E, Knauer SK, Schmuck C. Incorporation of a non-natural arginine analogue into a cyclic peptide leads to formation of positively charged nanofibers capable of gene transfection. Angew Chem Int Ed Engl 2016;55:598–601.
[61] Lee YH, Chang SF, Liaw J. Anti-apoptotic gene delivery with cyclo-(d-Trp-Tyr) peptide nanotube via eye drop following corneal epithelial debridement. Pharmaceutics 2015;7:122–36.
[62] Uji H, Kim H, Imai T, Mitani S, Sugiyama J, Kimura S. Electronic properties of tetrathiafulvalene-modified cyclic-β-peptide nanotube. Biopolymers 2016;106:275–82.
[63] Lee JS, Yoon I, Kim J, Ihee H, Kim B, Park CB. Self-assembly of semiconducting photoluminescent peptide nanowires in the vapor phase. Angew Chem Int Ed Engl 2011;50:1164–7.
[64] Patolsky F, Timko BP, Zheng G, Lieber CM. Nanowire-based nanoelectronic devices in the life sciences. MRS Bull 2007;32:142–9.
[65] Montenegro J, Ghadiri MR, Granja JR. Ion channel models based on self-assembling cyclic peptide nanotubes. Acc Chem Res 2013;46:2955–65.
[66] Yan X, Fan J, Yu Y, Xu J, Zhang M. Transport behavior of a single Ca(2+), K(+), and Na(+) in a water-filled transmembrane cyclic peptide nanotube. J Chem Inf Model 2015;55:998–1011.
[67] Zhang M, Fan J, Xu J, Weng P, Lin H. Different transport behaviors of NH4 (+) and NH3 in transmembrane cyclic peptide nanotubes. J Mol Model 2016;22:233.

[68] Liu J, Fan J, Tang M, Cen M, Yan J, Liu Z, et al. Water diffusion behaviors and transportation properties in transmembrane cyclic hexa-, octa- and decapeptide nanotubes. J Phys Chem B 2010;114:12183–92.
[69] Burade SS, Saha T, Bhuma N, Kumbhar N, Kotmale A, Rajamohanan PR, et al. Self-assembly of fluorinated sugar amino acid derived α,γ-cyclic peptides into transmembrane anion transport. Org Lett 2017;19:5948–51.
[70] Liu J, Fan J, Cen M, Song X, Liu D, Zhou W, et al. Dependences of water permeation through cyclic octa-peptide nanotubes on channel length and membrane thickness. J Chem Inf Model 2012;52:2132–8.
[71] Xu J, Fan JF, Zhang MM, Weng PP, Lin HF. Transport properties of simple organic molecules in a transmembrane cyclic peptide nanotube. J Mol Model 2016;22:107.
[72] Carvajal-Diaz JA, Cagin T. Electrophoretic transport of Na(+) and K(+) ions within cyclic peptide nanotubes. J Phys Chem B 2016;120:7872–9.
[73] Li H, Fan JF, Li R, Yu Y, Yan XL. Molecular dynamics studies on the influences of a gradient electric field on the water chain in a peptide nanotube. J Mol Model 2014;20:2370.
[74] Dehez F, Tarek M, Chipot C. Energetics of ion transport in a peptide nanotube. J Phys Chem B 2007;111:10633–5.
[75] Hwang H, Schatz GC, Ratner MA. Steered molecular dynamics studies of the potential of mean force of a Na+ or K+ ion in a cyclic peptide nanotube. J Phys Chem B 2006;110:26448–60.
[76] Song Y, Lee JH, Hwang H, Schatz GC, Hwang H. Energetic and dynamic analysis of transport of Na+ and K+ through a cyclic peptide nanotube in water and in lipid bilayers. J Phys Chem B 2016;120:11912–22.
[77] Song X, Fan J, Liu D, Li H, Li R. Molecular dynamics study of Na^+ transportation in a cyclic peptide nanotube and its influences on water behaviors in the tube. J Mol Model 2013;19:4271–82.
[78] Li R, Fan J, Li H, Yan X, Yu Y. Dynamic behaviors and transport properties of ethanol molecules in transmembrane cyclic peptide nanotubes. J Chem Phys 2015;143. 015101.
[79] Li R, Fan J, Li H, Yan X, Yu Y. Exploring the dynamic behaviors and transport properties of gas molecules in a transmembrane cyclic peptide nanotube. J Phys Chem B 2013;117:14916–27.
[80] Liu J, Fan J, Tang M, Zhou W. Molecular dynamics simulation for the structure of the water chain in a transmembrane peptide nanotube. J Phys Chem A 2010;114:2376–83.
[81] Clark TD, Buehler LK, Ghadiri MR. Self-assembling cyclic β3-peptide nanotubes as artificial transmembrane ion channels. J Am Chem Soc 1998;120:651–6.
[82] García-Fandiño R, Amorín M, Castedoa L, Granja JR. Transmembrane ion transport by self-assembling α,γ-peptide nanotubes. Chem Sci 2012;3:3280–5.